Electronic Supplementary Material (ESI) for Materials Horizons.

Are Formation and Adsorption Energies Enough to Evaluate the Stability of Surface-Passivated Tin-based Halide Perovskites?

Yapeng Zheng,[a,b] Zhi Fang,[a] Minghui Shang,[a,] Qian Sun,[a,b] Xinmei Hou[b,]* and Weiyou Yang[a,]**

[a] Institute of Micro/Nano Materials and Devices, Ningbo University of Technology, Ningbo City, 315211, P.R. China.

[b] Collaborative Innovation Center of Steel Technology, University of Science and Technology Beijing, Beijing, 100083, P. R. China.

Corresponding Author

* Minghui Shang, E-mail: shangminghui@nbut.edu.cn.

* Xinmei Hou, E-mail: houxinmeiustb@ustb.edu.cn.

* Weiyou Yang, E-mail: weiyouyang@tsinghua.org.cn.

Computational method

Density Functional Theory Calculation

The γ-$CsSnI_3$ (202) slab model terminated with Cs-I was constructed with 7 octahedral layers (*i.e.*, 15 atomic layers) and a 16 Å vacuum layer along normal direction based on our previous convergence test (Figure S1).[1, 2] The iodine anions at the surface of slab model were removed for modeling surface V_I, and pseudo-halide anions were situated at V_I to simulate passivated configurations. Based on the constructed models, first-principles calculations were performed by employing Vienna *ab*-initio simulation package (VASP) code.[3, 4] The Perdew-Burke-Ernzerhof (PBE) type of generalized gradient approximation (GGA) functional, which contains information about local electron density and local gradient in the electron density, was adopted to define the approximate exchange-correlation functional.[5] The pseudopotentials of elements were based on projector-augmented wave (PAW) method.[6] The long-range weak van der Waals interaction was treated by the Grimme's DFT-D3.[7, 8] The dipole correction along lattice *c* was implemented to remove additional field. The cutoff energy was set as 460 eV, and the Brillouin zone was sampled by a Monkhorst-Pack K-point mesh with grid of 3×5×1 after convergence test. The upper five atomic layers and pseudo-halide anions were fully relaxed and served as surface component, while the other atoms were fixed and simulated bulk component during the theoretical simulation. The convergency criteria of energy and Hellman-Feynman forces on individual atom were 1×10^{-4} eV/atom and 0.05 eV/Å, respectively.

Because the Cs, Pb and I are not the light elements that one can neglect relativistic spin-orbit coupling. The spin-orbital coupling (SOC) effect is introduced in typical γ-$CsSnI_3$ and *β*-$CsPbI_3$ passivated configuration, determining whether SOC effect would change the computational results based on PBE+SOC.

The van der Waals volume of pseudo-halide anions were calculated within the framework of density functional theory using the hybrid functional of B3LYP with a basis set 6-31+G* as implemented in the Gaussian16 program.

Ab-initio Molecular Dynamics

The *ab*-initio molecular dynamics (AIMD) simulations under 300 K were implemented to evaluate the stability of passivated configurations with low energy thermal excitation. The ensemble was chosen as NVT with a Nosé-Hoover thermostat.[9, 10] The time step and the

simulation time were set as 1 fs and 5 ps, respectively. The simulations were performed at the Γ-point, and the calculations of other parameters were performed based on above-mentioned method.

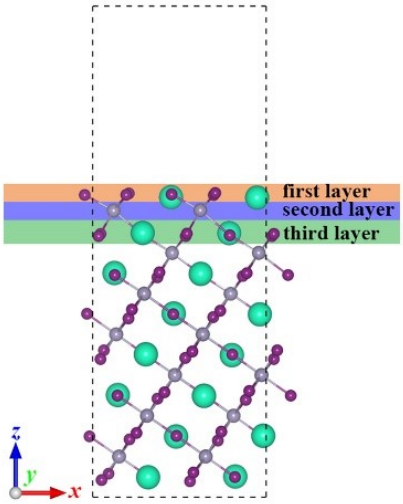

Figure S1. The schematic diagram of pristine γ-$CsSnI_3$ slab.

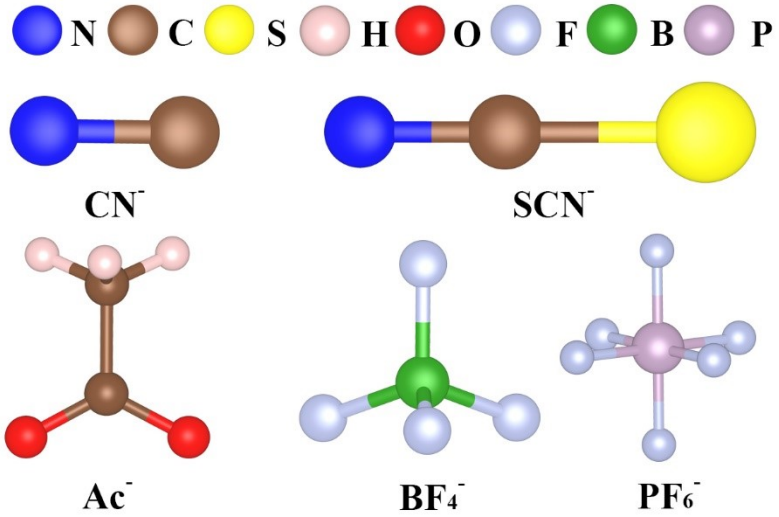

Figure S2. The structures of CN^-, SCN^-, Ac^-, BF_4^- and PF_6^- pseudo-halide anions.

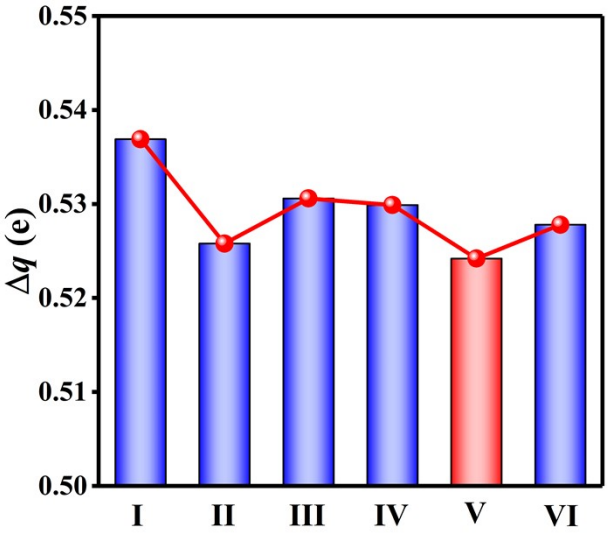

Figure S3. The net charges of six iodine anions at the first layer of pristine slab.

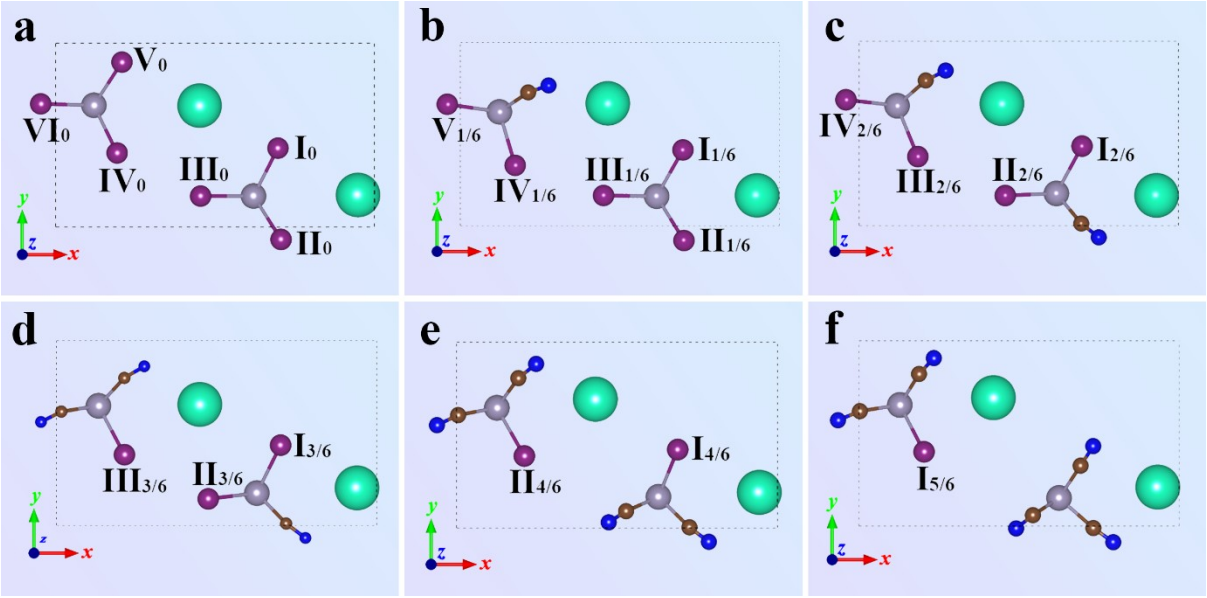

Figure S4. (a-f) The potential sites for the formation of surface V_I in CN^--passivated configurations with 0, 1/6, 2/6, 3/6, 4/6 and 5/6 ML coverages, respectively.

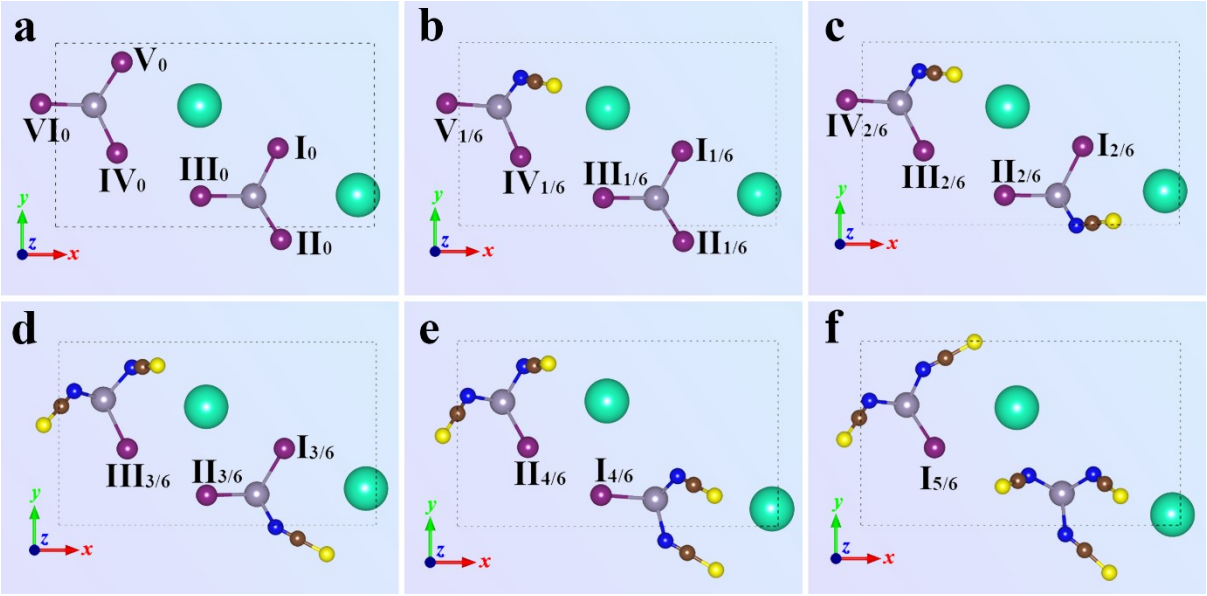

Figure S5. (a-f) The potential sites for the formation of surface V_I in SCN^--passivated configurations with 0, 1/6, 2/6, 3/6, 4/6 and 5/6 ML coverages, respectively.

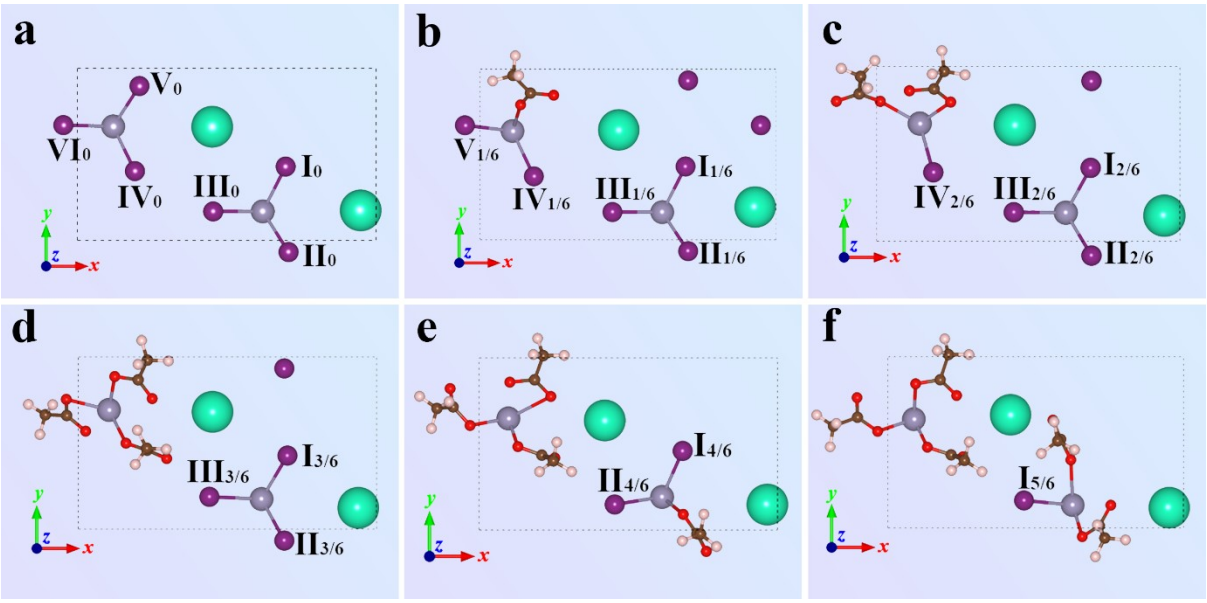

Figure S6. (a-f) The potential sites for the formation of surface V_I in Ac^--passivated configurations with 0, 1/6, 2/6, 3/6, 4/6 and 5/6 ML coverages, respectively.

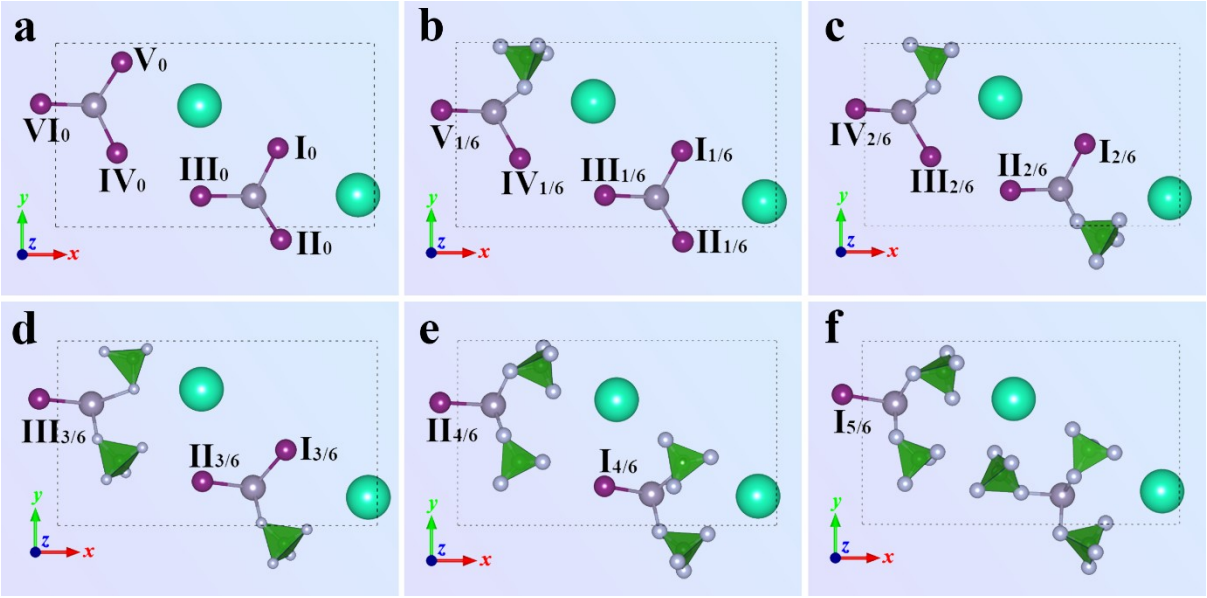

Figure S7. (a-f) The potential sites for the formation of surface V_I in BF_4^--passivated configurations with 0, 1/6, 2/6, 3/6, 4/6 and 5/6 ML coverages, respectively.

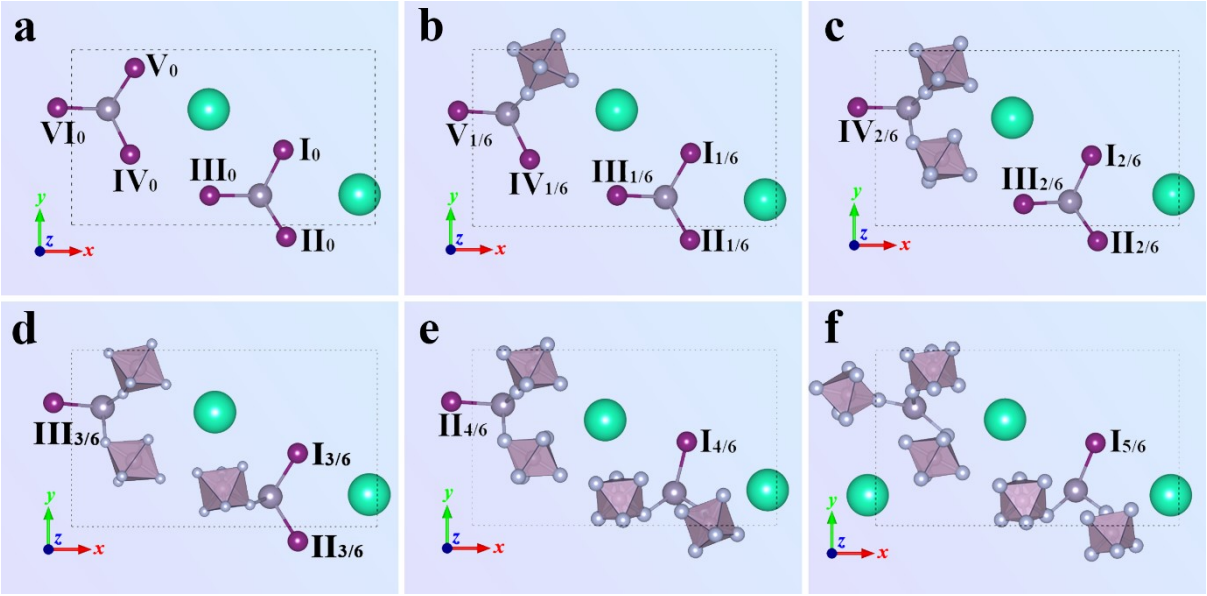

Figure S8. (a-f) The potential sites for the formation of surface V_I in PF_6^--passivated configurations with 0, 1/6, 2/6, 3/6, 4/6 and 5/6 ML coverages, respectively.

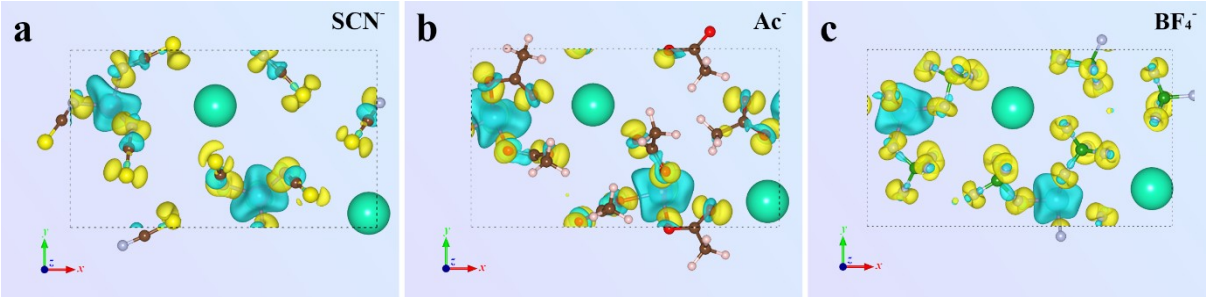

Figure S9. (a-c) The CDD between SCN^-, Ac^- and BF_4^- anions at the first atomic layer and inferior Sn cations, respectively. The yellow and blue isosurfaces set as 0.005 e/a_0^3 indicate the charge accumulation and depletion regions, respectively.

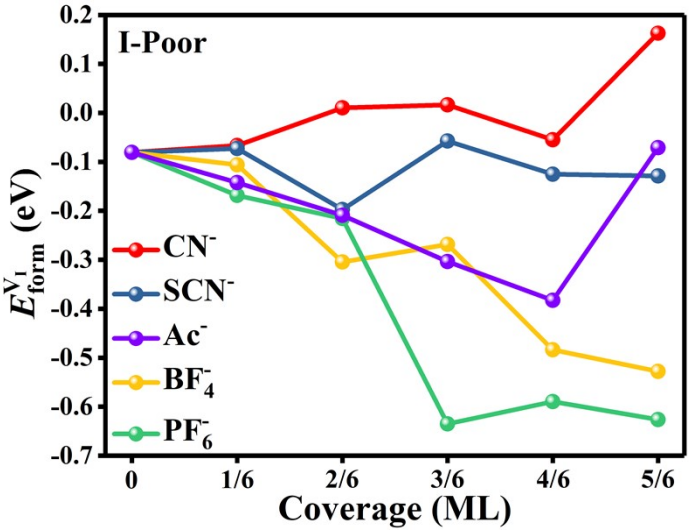

Figure S10. The $E^{V_I}_{form}$ of passivated configurations with different coverage under I-poor environment.

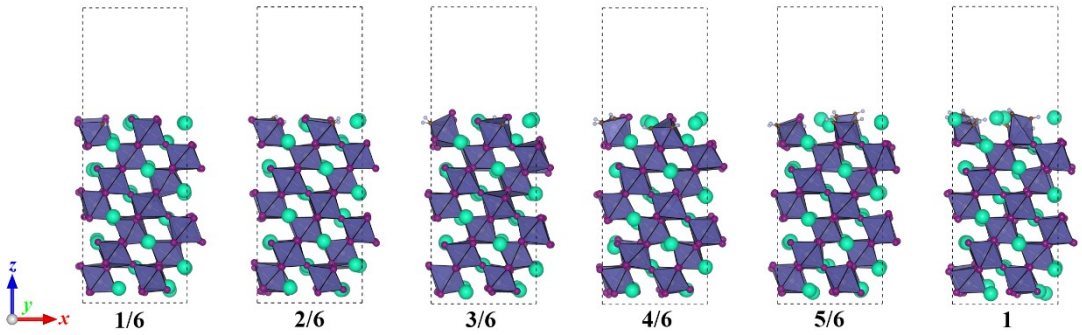

Figure S11. The structures of CN^--passivated configurations with different coverages after AIMD simulations.

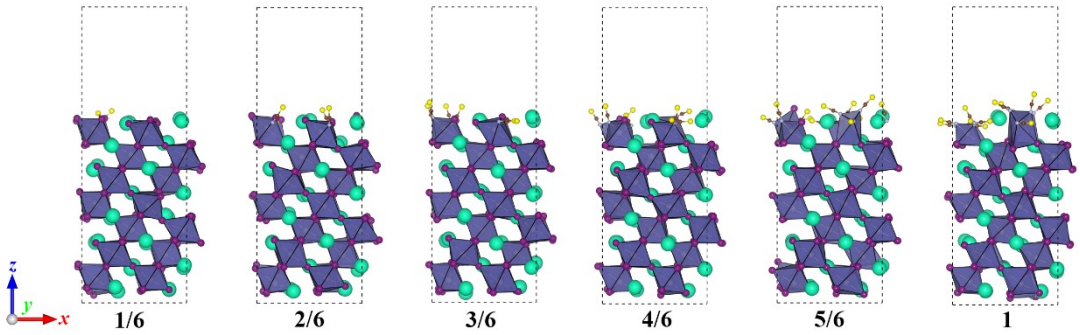

Figure S12. The structures of SCN^--passivated configurations with different coverages after AIMD simulations.

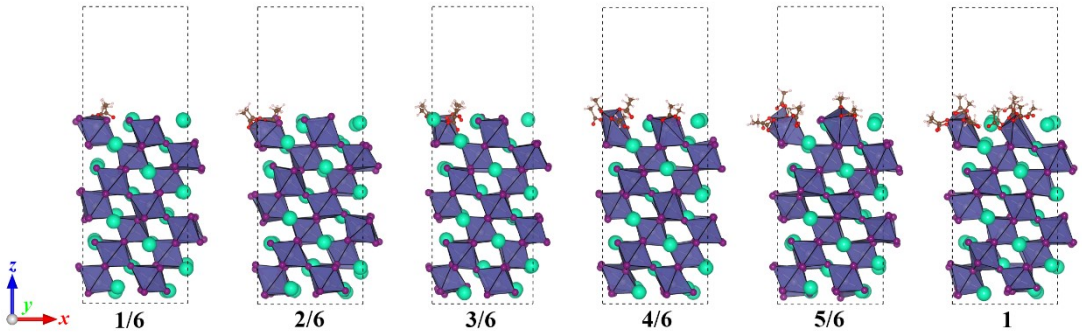

Figure S13. The structures of Ac^--passivated configurations with different coverages after AIMD simulations.

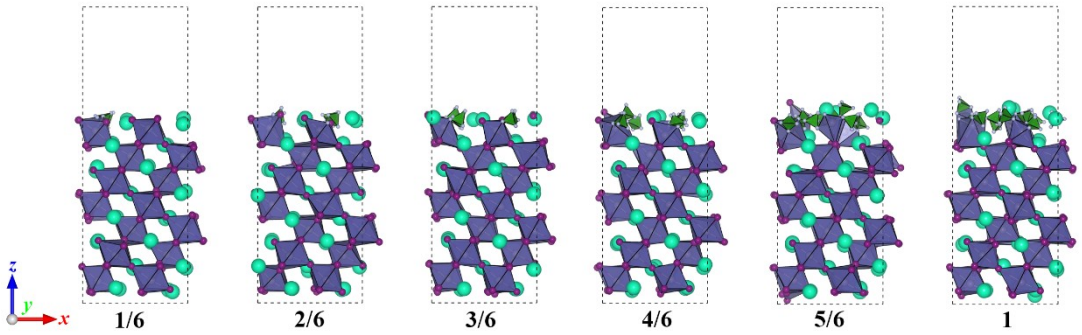

Figure S14. The structures of BF_4^--passivated configurations with different coverages after AIMD simulations.

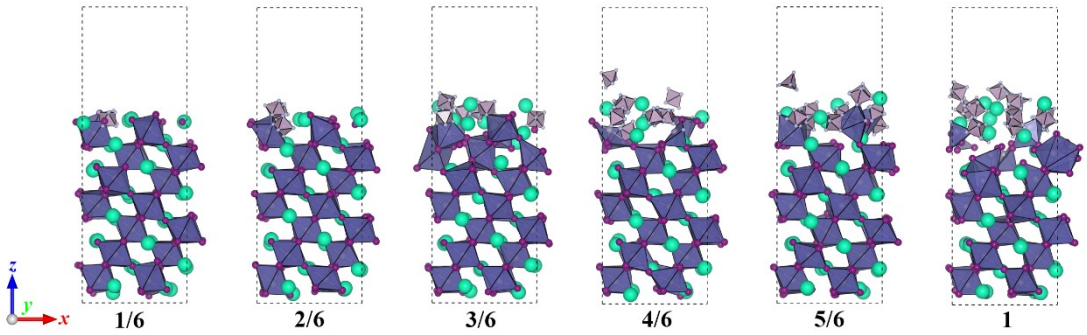

Figure S15. The structures of PF_6^--passivated configurations with different coverages after AIMD simulations.

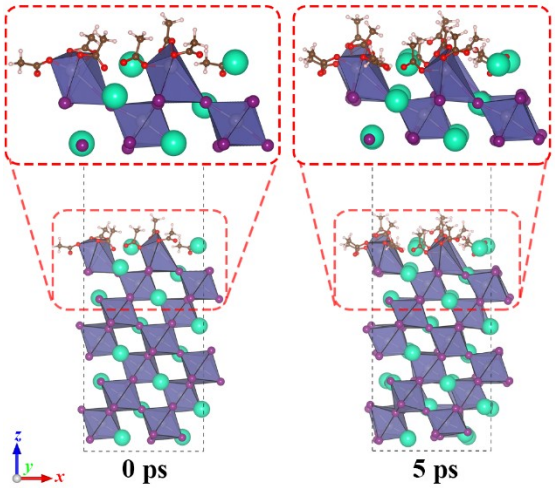

Figure S16. The structures and local surface structures of Ac^--passivated configurations recorded at 0 and 5 ps of AIMD simulations.

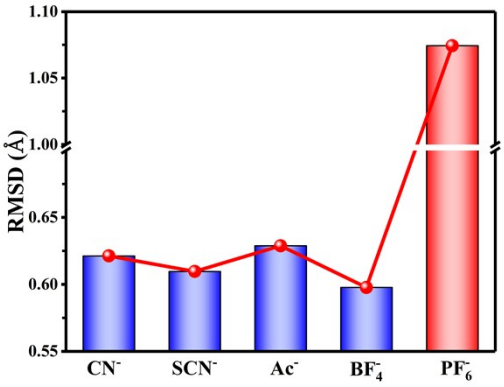

Figure S17. The RMSD of atoms within passivated configurations with 1 ML coverage, where the pseudohalide anions at the first atomic layer are not counted.

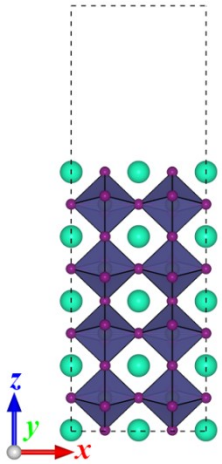

Figure S18. The schematic diagram of pristine β-$CsPbI_3$ slab.

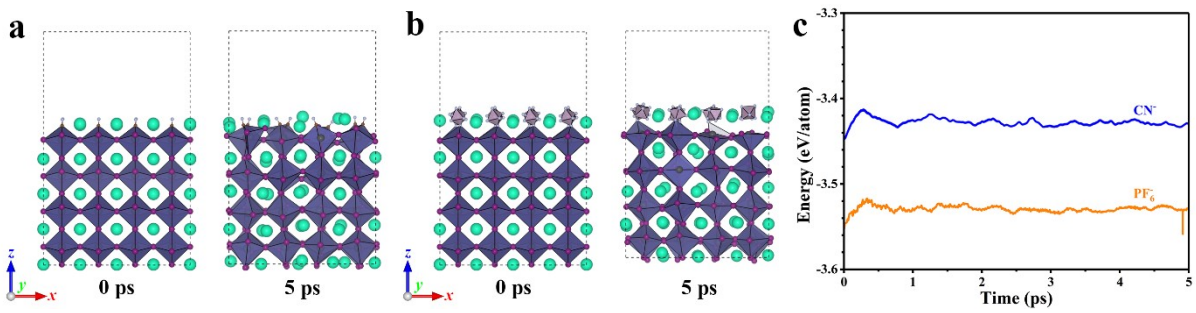

Figure S19. (a, b) The structures of β-$CsPbI_3$ surface models passivated by CN^- and PF_6^- recorded at 0 and 5 ps of AIMD simulations, respectively. (c) The energies vs. relaxing times as results of thermal effect simulated by AIMD.

Table S1. The $E_{form}^{V_I}$ of pristine γ-$CsSnI_3$ slab under I-rich and I-poor environment.

	I	II	III	IV	V	VI
I-rich	0.660	0.620	0.728	0.671	**0.620**	0.719
I-poor	-0.040	-0.080	0.028	-0.029	**-0.080**	0.019

Table S2. The $E_{form}^{V_I}$ of CN^--passivated configurations with 1/6, 2/6, 3/6, 4/6 and 5/6 ML coverage under I-rich environment.

***x* (coverage, ML)**	I_x	II_x	III_x	IV_x	V_x
1/6	0.739	**0.634**	0.658	0.708	0.709
2/6	0.794	0.722	0.775	**0.710**	
3/6	0.752	**0.716**	0.816		
4/6	**0.645**	0.5914			
5/6	**0.863**				

Table S3. The $E_{\text{form}}^{V_I}$ of CN^--passivated configurations with 1/6, 2/6, 3/6, 4/6 and 5/6 ML coverage under I-poor environment.

***x* (coverage, ML)**	I_x	II_x	III_x	IV_x	V_x
1/6	0.039	**-0.066**	-0.042	0.008	0.009
2/6	0.094	0.022	0.075	**0.010**	
3/6	0.062	**0.016**	0.116		
4/6	**-0.055**	0.214			
5/6	**0.163**				

Table S4. The $E_{\mathrm{form}}^{\mathrm{V_I}}$ of SCN^--passivated configurations with 1/6, 2/6, 3/6, 4/6 and 5/6 ML coverage under I-rich environment.

***x* (coverage, ML)**	I_x	II_x	III_x	IV_x	V_x
1/6	0.645	**0.628**	0.708	0.685	0.716
2/6	0.655	0.516	0.664	**0.503**	
3/6	**0.643**	0.732	0.663		
4/6	**0.575**	0.636			
5/6	**0.571**				

Table S5. The $E_{\mathrm{form}}^{\mathrm{V_I}}$ of SCN^--passivated configurations with 1/6, 2/6, 3/6, 4/6 and 5/6 ML coverage under I-poor environment.

***x* (coverage, ML)**	I_x	II_x	III_x	IV_x	V_x
1/6	-0.055	**-0.072**	0.008	-0.015	0.016
2/6	-0.045	-0.184	-0.036	**-0.197**	
3/6	**-0.057**	0.031	-0.037		
4/6	**-0.125**	-0.064			
5/6	**-0.129**				

Table S6. The $E_{\text{form}}^{\text{V}_\text{I}}$ of Ac^--passivated configurations with 1/6, 2/6, 3/6, 4/6 and 5/6 ML coverage under I-rich environment.

***x* (coverage, ML)**	I_x	II_x	III_x	IV_x	V_x
1/6	0.594	0.579	0.759	0.598	**0.558**
2/6	0.687	0.627	0.746	**0.491**	
3/6	0.500	**0.397**	0.558		
4/6	**0.317**	0.426			
5/6	**0.629**				

Table S7. The $E_{\text{form}}^{\text{V}_\text{I}}$ of Ac^--passivated configurations with 1/6, 2/6, 3/6, 4/6 and 5/6 ML coverage under I-poor environment.

***x* (coverage, ML)**	I_x	II_x	III_x	IV_x	V_x
1/6	-0.106	-0.121	0.059	-0.102	**-0.142**
2/6	-0.013	-0.073	0.046	**-0.209**	
3/6	-0.200	**-0.303**	-0.142		
4/6	**-0.383**	-0.274			
5/6	**-0.071**				

Table S8. The $E_{\mathrm{form}}^{\mathrm{V_I}}$ of BF_4^--passivated configurations with 1/6, 2/6, 3/6, 4/6 and 5/6 ML coverage under I-rich environment.

***x* (coverage, ML)**	I_x	II_x	III_x	IV_x	V_x
1/6	0.594	**0.594**	0.614	0.656	0.679
2/6	0.429	0.534	**0.396**	0.531	
3/6	**0.432**	0.533	0.549		
4/6	**0.216**	0.223			
5/6	**0.172**				

Table S9. The $E_{\text{form}}^{V_I}$ of BF_4^--passivated configurations with 1/6, 2/6, 3/6, 4/6 and 5/6 ML coverage under I-poor environment.

***x* (coverage, ML)**	I_x	II_x	III_x	IV_x	V_x
1/6	-0.106	**-0.106**	-0.086	-0.044	-0.021
2/6	-0.271	-0.166	**-0.305**	-0.169	
3/6	**-0.268**	-0.167	-0.151		
4/6	**-0.484**	-0.477			
5/6	**-0.528**				

Table S10. The $E_{\mathrm{form}}^{\mathrm{V_I}}$ of PF_6^--passivated configurations with 1/6, 2/6, 3/6, 4/6 and 5/6 ML coverage under I-rich environment.

***x* (coverage, ML)**	I_x	II_x	III_x	IV_x	V_x
1/6	0.663	0.618	0.614	**0.532**	0.687
2/6	0.673	0.485	**0.484**	0.592	
3/6	0.452	**0.065**	0.217		
4/6	0.327	**0.111**			
5/6	**0.074**				

Table S11. The $E_{\mathrm{form}}^{\mathrm{V_I}}$ of PF_6^--passivated configurations with 1/6, 2/6, 3/6, 4/6 and 5/6 ML coverage under I-poor environment.

***x* (coverage, ML)**	I_x	II_x	III_x	IV_x	V_x
1/6	-0.037	-0.082	-0.086	**-0.168**	-0.013
2/6	-0.027	-0.215	**-0.216**	-0.108	
3/6	-0.247	**-0.635**	-0.483		
4/6	-0.373	**-0.589**			
5/6	**-0.626**				

Table S12. E_{form} of CN^-, SCN^- and PF_6^--passivated configurations based on PBE+SOC.

Passivated Configurations	E_{form} (eV/atom)
CN^-	-1.13
SCN^-	-1.07
PF_6^-	-1.24

Table S13. The calculated vdW volume of pseudo-halide anions.

Pseudo-halide Anions	CN^-	SCN^-	Ac^-	BF_4^-	PF_6^-
Volume ($Å^3$)	53.71	80.96	86.18	72.39	98.29

Table S14. The main X-ray diffraction peaks of bulk β-$CsPbI_3$.

Main Diffraction Peaks	Reference
(220) (110) (002)	11
(220) (110) (111)	12
(220) (110) (002)	13
(220) (110)	14

Table S15. Surface energies of β-$CsPbI_3$ slab with Sn and Cs-I terminal ions.

Termination	Surface Energies (meV/Å^2)
Pb-I	6.2
Cs-I	2.6

Table S16. E_{form} of β-$CsPbI_3$ slab passivated by CN^- and PF_6^- based on PBE+SOC.

Passivated Configurations	E_{form} (eV/atom)
CN^-	-1.12
PF_6^-	-1.21

Table S17. The average |ICOHP| of Pb_2-I_3 within pristine β-$CsPbI_3$ slab and the counterpart passivated by CN^- and PF_6^-.

	|ICOHP| (eV)
Pristine slab	1.21
CN^--passivated configuration	1.00
PF_6^--passivated configuration	1.91

Reference:

1 Y. Zheng, Z. Fang, M.-H. Shang, Z. Du, Z. Yang, K.-C. Chou, W. Yang, S. Wei and X. Hou, *ACS Appl. Mater. Interfaces,* 2020, **12**, 34462-34469.

2 Y. Zheng, Z. Fang, M. Shang, Q. Sun, J. Zheng, Z. Yang, X. Hou and W. Yang, *ACS Energy Lett.* , 2021, **6**, 2328-2335.

3 G. Kresse and J. Hafner, *Phys. Rev. B*, 1993, **48**, 13115-13118.

4 G. Kresse and J. Furthmüller, *Phys. Rev. B*, 1996, **54**, 11169-11186.

5 J. P. Perdew, K. Burke and M. Ernzerhof, *Phys. Rev. Lett.* , 1996, **77**, 3865-3868.

6 P. E. Blöchl, *Phys. Rev. B*, 1994, **50**, 17953-17979.

7 S. Grimme, J. Antony, S. Ehrlich and H. Krieg, *J. Chem. Phys.* , 2010, **132**, 154104.

8 S. Grimme, S. Ehrlich and L. Goerigk, *J. Comput. Chem.* , 2011, **32**, 1456-1465.

9 S. Nosé, *J. Chem. Phys.* , 1984, **81**, 511-519.

10 G. J. Martyna, M. L. Klein and M. Tuckerman, *J. Chem. Phys.* , 1992, **97**, 2635-2643.

11 Y. Wang, M. I. Dar, L. K. Ono, T. Zhang, M. Kan, Y. Li, L. Zhang, X. Wang, Y. Yang, X. Gao, Y. Qi, M. Grätzel and Y. Zhao, *Science*, 2019, **365**, 591-595.

12 H. Li, H. Lin, D. Ouyang, C. Yao, C. Li, J. Sun, Y. Song, Y. Wang, Y. Yan, Y. Wang, Q. Dong and W. C. H. Choy, *Adv. Mater.* , 2021, **33**, 2008820.

13 K. Wang, Q. Tian, G. Zhao, J. Wen, J. Huang, C. Gao, Z. Xu, Y. Liu, L. Liang, L. Meng, L. Zhang, Z. Liu, Z. Jin, S. Olthof and S. Liu, *Cell Reports Physical Science*, 2020, **1**, 100180.

14 Y. Wang, X. Liu, T. Zhang, X. Wang, M. Kan, J. Shi and Y. Zhao, *Angew. Chem. Int. Ed.* , 2019, **58**, 16691-16696.